




Open Archive Toulouse Archive Ouverte (OATAO)

OATAO is an open access repository that collects the work of Toulouse researchers and makes it freely available over the web where possible

This is an author's version published in: <http://oatao.univ-toulouse.fr/23665>

Official URL: <https://doi.org/10.1007/s11085-013-9382-2>

To cite this version:

Dryepondt, Sebastien and Vande Put, Aurélie  and Pint, Bruce A. *Effect of H₂O and CO₂ on the Oxidation Behavior and Durability at High Temperature of ODS-FeCrAl*. (2013) *Oxidation of Metals*, 79 (5-6). 627-638. ISSN 0030-770X

Any correspondence concerning this service should be sent to the repository administrator: tech-oatao@listes-diff.inp-toulouse.fr

Effect of H₂O and CO₂ on the Oxidation Behavior and Durability at High Temperature of ODS-FeCrAl

Sebastien Dryepondt · Aurelie Rouaix-Vande Put ·
Bruce A. Pint

Abstract Cyclic oxidation testing was conducted on alloy MA956 and two different batches of alloy PM2000 at 1,100 and 1,200 °C in different atmospheres rich in O₂, H₂O and CO₂. Compared to 1 h cycles in dry O₂, exposure in air + 10 vol.% H₂O resulted in an increase of the oxidation rate and a decrease of the time to breakaway for all alloys at 1,200 °C, and a faster consumption of Al in the MA956 alloy. One hour cyclic testing in 49.25 % CO₂ + 50 % H₂O + 0.75 % O₂ had a smaller effect on the oxidation rate but led to increased formation of voids in alloy MA956, which had an impact on the alloy creep resistance. At 1,100 °C, exposure in 50 % CO₂ + 50 % H₂O resulted in significant oxide spallation compared with oxidation in air, but this was not the case when 0.75 % O₂ was added to the CO₂/H₂O mixture as a buffer. The control of impurity levels drastically improved the oxidation resistance of PM2000.

Keywords ODS alloys · Lifetime · H₂O · CO₂

Introduction

Oxide dispersion strengthened (ODS) alloys are of great interest for high-temperature applications because of their excellent creep and oxidation resistance

S. Dryepondt (✉) · B. A. Pint
Oak Ridge National Laboratory, 1 Bethel Valley Road, 37831 Oak Ridge, TN, USA
e mail: dryepondtsn@ornl.gov

B. A. Pint
e mail: pintba@ornl.gov

A. Rouaix Vande Put
Institut Carnot CIRIMAT, ENSIACET, 4 Allée Emile Monso, BP 44362, 31432 Toulouse Cedex 4,
France
e mail: aurelie.rouaix@ensiacet.fr

at temperatures up to 1,200 °C [1]. The presence of nano-oxide particles, 20–50 nm average diameter, results in the existence of a temperature-dependent stress threshold below which the minimum creep rate is very low and the time to rupture reaches thousands of hours. For well-designed components, lifetime is therefore expected to depend on the alloy oxidation resistance, and lifetime models based on oxidation kinetics have been developed [2, 3]. These models considered that the lifetime is dictated by the consumption of Al from the alloy to form an alumina scale to a point where the Al level is insufficient to maintain alumina formation and fast-growing Fe-rich oxides start to form. The model proposed by Quadackers et al. [2] was based on the following relation:

$$1.125 \cdot k \cdot t_b^n = \frac{C_0 - C_b}{100} \cdot \rho \cdot \frac{d}{2} \quad (1)$$

where 1.125 is the Al/O-mass ratio in alumina, k and n are parameters related to the oxidation kinetics, d is the thickness of the specimen, ρ is the alloy density, C_0 is the initial Al content (in wt%), C_b is the Al content at the onset of breakaway oxidation and t_b is the time to breakaway. The addition of H₂O to the environment was found to decrease the time to breakaway [4, 5], without affecting C_b [4]. Recent work on MA956 ODS FeCrAl alloy [6] confirmed the effect of H₂O on the lifetime and highlighted a possible change in C_b with the environment. H₂O has been reported to have various effects on the oxidation behavior of alumina-forming materials. For example, Janakiraman et al. [7] showed that H₂O often decreased the adherence of alumina scales formed on Ni-based alloys, but had no effect on scale spallation when the metal/oxide interfacial toughness was sufficiently high. Hayashi and Narita observed an effect of the H₂O/O₂ ratio on the mass changes obtained during the oxidation of Fe–5Al alloy in N₂–O₂–12.2H₂O atmospheres [8], and Maris-Sida et al. [9] noticed that higher H₂O levels led to larger spallation on the René N5 superalloy, which was later confirmed by Pint et al. [10] for Ni–Pt–Al coatings. In a 50% CO₂ + 50% H₂O environment, Pint and Wright [11] reported increased scale spallation and oxidation rate for MA956 alloy subjected to 500 h cycles at 1,100 °C compared to exposure in air, whereas Vande Put et al. [6] observed similar lifetimes in O₂ and CO₂ + 50% H₂O with O₂ added as a buffer, for the same material subjected to 1 h cycles at 1,200 °C. In the latter study, a reduction in C_b was measured.

To follow up on this prior work, experiments have been performed on ODS alloys at 1,100 and 1,200 °C in different O₂, H₂O, CO₂ environments. The effect of H₂O and CO₂ on the oxidation kinetics, spallation rates and specimen lifetimes will be discussed. Scanning electron microscopy (SEM) and electron probe microanalysis (EPMA) characterization was also used to assess the role played by the environment on the alloy microstructure evolution, mainly on the Al gradient and porosity formation in the alloy. Moreover, to assess the impact of oxidation on the alloy mechanical properties, small creep specimens were exposed to O₂ and CO₂–H₂O-rich environments prior to creep testing in air.

Experimental Procedures

Three different ODS alloys were used for this study: alloy MA956 (69.45 Fe, 20.07 Cr, 8.78 Al, 0.13 Si, 0.4 Ti, 0.24 Y, 0.064 C, 0.06 N, 0.649 O, 0.0041 S, at.%) provided by Special Metals Corp. (Huntington, West Virginia) and two versions of alloy PM2000, designated PM2000 (69.4 Fe, 18.91 Cr, 9.82 Al, 0.07 Si, 0.49 Ti, 0.22 Y, 0.043 C, 0.01 N, 0.805 O, 0.0034 S, at.%) and PM2K (68.7 Fe, 19.05 Cr, 10.48 Al, 0.037 Si, 0.52 Ti, 0.23 Y, 0.006 C, 0.031 N, 0.803 O, 0.0013 S, at.%) provided by Metalwerk Plansee (Reutte, Austria).

Rectangular coupons $\sim 18 \times 10 \times 0.5$ mm were machined from plate or rod (PM2K) in the fully recrystallized condition, resulting in specimens with a three-grain microstructure for the MA956 and PM2000 coupons, and a monocrystalline structure for the PM2K coupons. Cyclic oxidation was conducted in air at 1,100 °C with 100 h cycles using box furnaces. Individual coupons were placed in alumina crucibles to measure both the mass of the specimen and the spalled oxides. For 50 % CO₂ + 50 % H₂O, with or without 0.75 % O₂ (exact composition with O₂ is 49.25 % CO₂ + 50 % H₂O + 0.75 % O₂ and is called O₂-buffered 50 % CO₂ + 50 % H₂O), 500 h cycles were carried out at 1,100 °C in a sealed (alumina) tube furnace. To accelerate specimen degradation, specimens were also cyclically tested at 1,200 °C, with a 1 h hot dwell and a 10 min cooling at ambient temperature, in O₂, air + 10 % H₂O or O₂-buffered 50 % CO₂ + 50 % H₂O.

Selected specimens were copper plated and cross-sectioned along the specimen length. The microstructure was characterized by optical and scanning electron microscopy, and Al profiles were obtained using a JEOL 8200 electron microprobe. Measurements of the room-temperature residual stress in the oxide scale were performed using the photo-stimulated piezo-spectroscopy (PSLS) technique. For creep testing at 1,100 °C, 25 mm-long dog bone specimens, with a gage length of ~ 8 mm and section of 2×2 mm², were machined and creep tested in the as received condition, and after 500, 1 h cycles in O₂ or O₂-buffered 50 % CO₂ + 50 % H₂O.

Results

Oxidation Behavior at 1,100 and 1,200 °C

The 100 h-cycle mass gains at 1,100 °C in laboratory air for MA956, PM2000 and PM2K are shown in Fig. 1a. The total mass changes, specimen plus spalled oxide, were very similar for the MA956 and PM2000 specimens and increased linearly with time after $\sim 1,000$ h. Specimen mass changes were also nearly identical for up to 5,000 h, but for longer durations, the PM2000 specimen started to lose mass (scale spallation) while the MA956 specimen continued to gain mass, again linearly with time. This could be explained by a difference in oxide scale degradation, occurring mainly by cracking and debonding for alloy MA956, with the oxide scale still locally attached, and by spallation and separation for PM2000. Overall, the two degradation modes led to similar oxidation kinetics. Oxidation testing of alloy

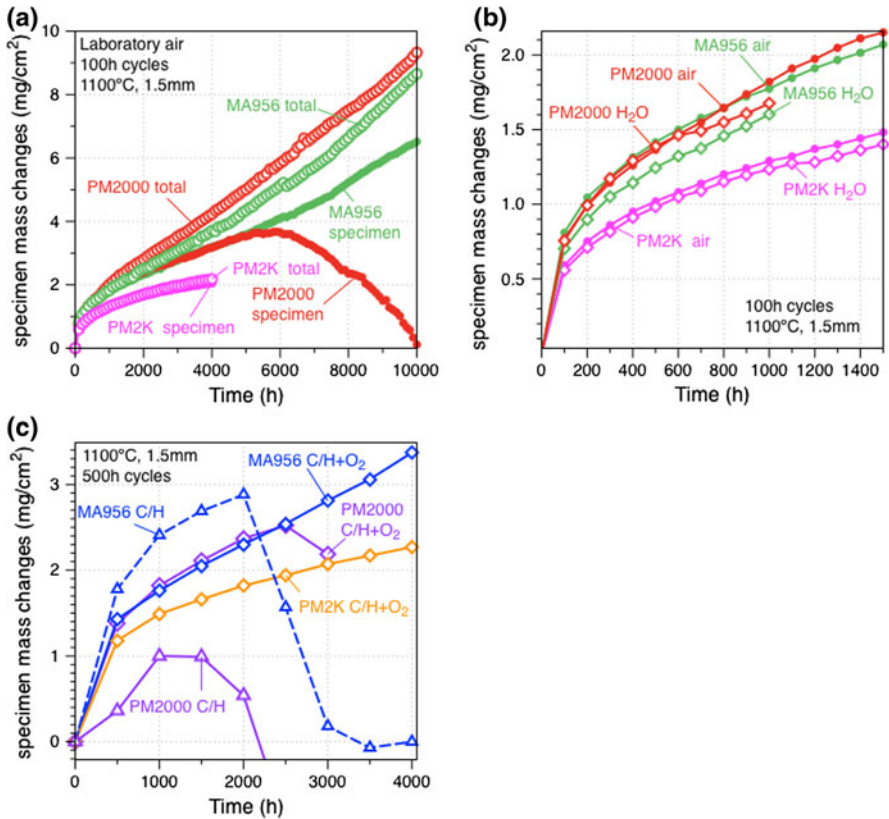


Fig. 1 Mass changes versus time for MA956, PM2000 and PM2K specimens (1.5 mm thickness) at 1,100 °C for **a** 100 h cycles in laboratory air, specimen and total (specimen + spalled oxides) mass changes, **b** 100 h cycles in laboratory air and air + 10 % H₂O, specimen mass changes **c** 500 h cycles in 50 % CO₂ + 50 % H₂O, O₂ buffered (C/H + O₂) and without O₂ (C/H), specimen mass changes

PM2K is on-going and has reached only 4,000 h, but the alloy has exhibited lower mass gain behavior with parabolic kinetics compared with the linear kinetics observed for the other alloys. The total and specimen mass changes were very similar, and inspection of the specimen surface revealed spallation occurred only at the specimen edges after 4,000 h.

As can be seen in Fig. 1b, 100 h cycles exposure in air + 10 % H₂O had little effect on the specimen mass gains after exposure for 1,000 h for alloy MA956 and PM2000, and 1,500 h for alloy PM2K. Surface observations after 1,000 h revealed also that the scales formed in air and air + 10 % H₂O were very similar, with very little spallation limited to the specimen edges and grain boundaries.

The curves in Fig. 1c compare 500 h cyclic testing in a mixture of 50 % CO₂ + 50 % H₂O, with and without the O₂ buffer. For the MA956 and PM2K alloys, exposure in O₂-buffered 50 % CO₂ + 50 % H₂O resulted in specimen mass changes similar to those observed in air, Fig. 1a. However, the

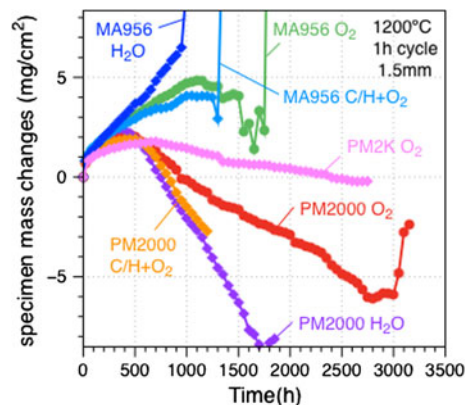
cycle duration was longer (500 vs. 100 h) leading to fewer cooling periods where spallation would be expected. The PM2000 alloy exhibited a different behavior, with spallation of nearly the entire oxide scale covering the bottom grain (Fig. 3c). The MA956 and PM2000 specimen mass change curves differed greatly when exposed to the 50 % CO₂ + 50 % H₂O without O₂, and significant spallation was observed on multiple (4) coupons of each alloy.

To accelerate specimen degradation and reach breakaway oxidation in shorter exposure times, specimens were exposed to 1 h cycles at 1,200 °C. The resulting specimen mass changes versus time are shown in Fig. 2. Again, specimen mass changes for MA956 and PM2000 were similar at the beginning. However, after 500 cycles, the PM2000 specimen started to lose mass at a constant rate while the MA956 alloy continued to gain mass, also at a constant rate. After 1,100 cycles for MA956 and 2,700 cycles for PM2000, spallation was more chaotic prior to the mass gain at the onset of breakaway oxidation. Similar to observations at 1,100 °C, the oxidation rate for alloy PM2K was slower, with little spallation and a curve shape similar to PM2000. However, significant mass loss occurred after 800 cycles, with a linear mass loss rate three times lower compared with alloy PM2000. The excellent oxidation resistance of the PM2K alloy is likely due to the high level of aluminum (10.48 at.%) and the very low level of S (13 ppm), an element that is known to affect oxide scale adhesion [12].

The MA956 and PM2000 were also exposed to 1 h cycles at 1,200 °C in air + 10 % H₂O and the O₂-buffered 50 % CO₂ + 50 % H₂O mixture, Fig. 2. Contrary to observations at 1,100 °C with 100 h cycles, Fig. 1b, acceleration of the oxidation rate was observed in air + 10 % H₂O for both alloys, i.e. increased specimen mass gains for MA956 and greater mass losses for PM2000. These results indicate that H₂O does not affect the growth of the alumina scale but enhances the scale spallation, as was observed previously [9, 10, 13].

The specimen mass change curve for the MA956 specimen in O₂-buffered 50 % CO₂ + 50 % H₂O was close to the curve obtained in O₂ but breakaway oxidation occurred sooner. In the case of PM2000, the alloy exhibited similar behavior in wet air and O₂-buffered CO₂ H₂O. To illustrate the effect of the alloy

Fig. 2 Specimen mass changes versus time for 1.5 mm thick MA956, PM2K and PM2000 specimens in 1 h cycles at 1,200 °C exposed in O₂, air + 10 % H₂O (H₂O) and O₂ buffered 50 % CO₂ + 50 % H₂O (C/H + O₂)



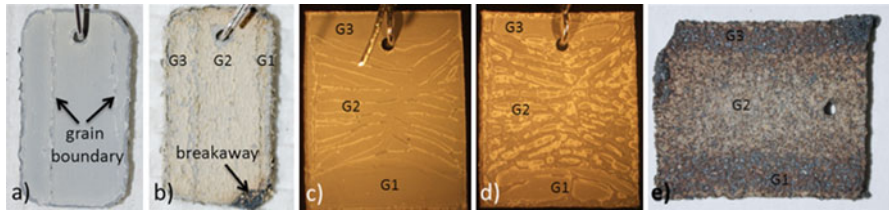


Fig. 3 Optical pictures of specimen surfaces after 1 h cycles at 1,200 °C, **a, b** MA956 specimens exposed in air + 10 % H₂O, after 550 and 1,000 cycles respectively, **c e** PM2000 specimens exposed in O₂ for 300, 800 and 3,150 cycles respectively. Alloy grains (G1–G3) are identified

grain structure, Fig. 3 compares macroscopic images of the cycled specimens. For a significant fraction of life, the specimens exhibited spallation patterns related to the grain structure and specimen geometry, Fig. 3a, c, d. For MA956, the scale was also more rumpled in the grain at the center, Fig. 3b. For longer exposure times, spallation was more random, but the grain structure was still apparent, Fig. 3b, e. A specific spallation pattern was also observed for PM2K, Fig. 4a, b. Stress mapping of the alumina scale by PSLS (Fig. 4c) illustrated the release of stress in the oxide scale by spallation and/or cracking at the specimen edges. This is especially true for creep-resistant ODS substrates that do not deform like FeCrAlY. For a significant fraction of the specimen lifetime, spallation cannot be considered as a statistically random process, but is directly related to the specimen geometry and grain structure and the development of stress in the scale.

Specimen Lifetimes with 1 h Cycles at 1,200 °C

MA956 and PM2000 specimens of thicknesses ranging from 0.5 to 2 mm were exposed until breakaway in O₂, air + 10 % H₂O and the O₂-buffered 50 % CO₂ + 50 % H₂O mixture, Fig. 5. The lifetime increased nearly linearly with specimen thickness, for both alloys in all three environments. Therefore, the exponent n in Eq. 1 is ~ 1 , which implies that the long-term oxidation rate is

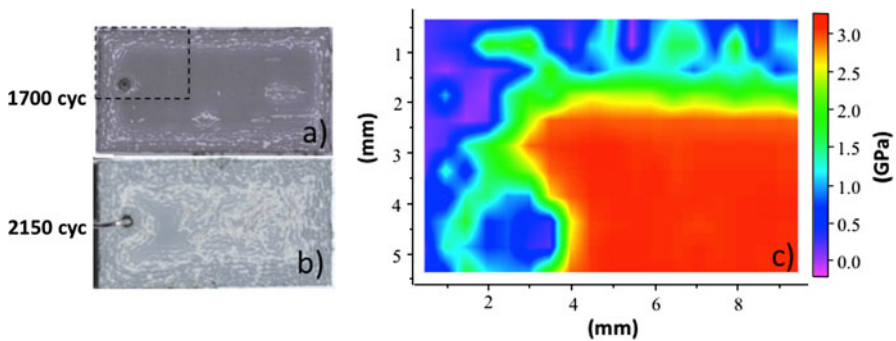
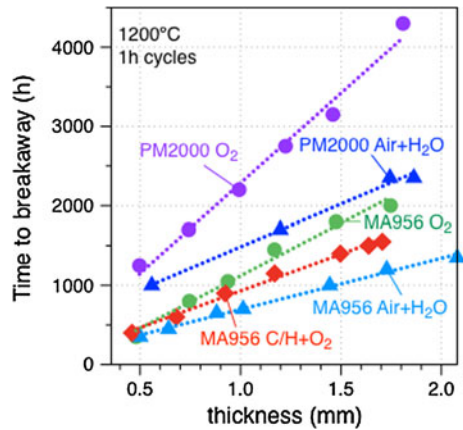


Fig. 4 PM2K specimens 1 h cycled at 1,200 °C in O₂, **a, b** optical pictures of the specimen surface exposed for 1,700 and 2,150 cycles respectively, **c** mapping of the residual stresses in the alumina scale by photo stimulated luminescence spectroscopy for the *box area* in picture (a)

Fig. 5 a Time to breakaway oxidation versus specimen thickness for alloy MA956 exposed in O₂, air + 10 % H₂O (H₂O) and O₂ buffered 50 % CO₂ + 50 % H₂O mixture (C/H + O₂) and alloy PM2000 exposed in O₂ and air + 10 % H₂O (H₂O)



dominated by scale spallation and follows a linear law, as was observed at 1,100 °C, Fig. 1a. Figure 5 also confirms a significant lifetime decrease due to exposure in humid air, a reduction that increased with increasing specimen thickness. As expected from the mass gain data, the O₂-buffered 50 % CO₂ + 50 % H₂O lifetimes lie between the trend lines relative to the O₂ and air + 10 % H₂O atmospheres.

After breakaway, MA956 specimens were cross-sectioned along the specimen length and the remaining Al content was measured along this direction using EPMA line scans, Fig. 6a, b. Figure 6c shows the Al profiles after various exposures in O₂ and air + 10 % H₂O and breakaway after 1,800 and 1,000 cycles respectively. The specific shape observed for the remaining Al content after breakaway in O₂ was due to the formation of a large population of AlN precipitates at the end of the specimen life, therefore depleting the matrix in Al. N is likely to come from exposure in air during cooling of the specimens.

Specimens were stopped at shorter times to understand the evolution of the Al profiles and consumption behavior. After 500 cycles at 1,200 °C (28 % of O₂ lifetime and 50 % in wet air), very similar Al profiles were measured in O₂ and air + 10 % H₂O. However, after 900 cycles (50 % of O₂ lifetime and 90 % in wet air) the remaining Al content was around 1.5 at.% in average lower after exposure in air + 10 % H₂O compared to O₂ but the profiles still exhibited the same shape, rather flat with small gradients at the edges. The Al content remaining after failure in O₂ strongly differed from that measured after 90 % of the lifetime (1,700 cycles), which was not the case with the air + 10 % H₂O atmosphere. The specimen tested for 1,700 cycles in O₂ exhibited localized internal oxidation. This specimen was therefore close to breakaway oxidation, which confirms that the significant difference between the Al profiles of the specimen stopped before and after breakaway oxidation is likely due to the trapping of Al in AlN precipitates.

Concentration gradients are usually measured in oxidized specimens when the consumption by selective oxidation of Al (or Cr and Si) is not totally compensated by an Al flux from the specimen center. However, for temperatures >1,100 °C, very small Al gradients were observed previously for alloys PM2000 and MA956 along

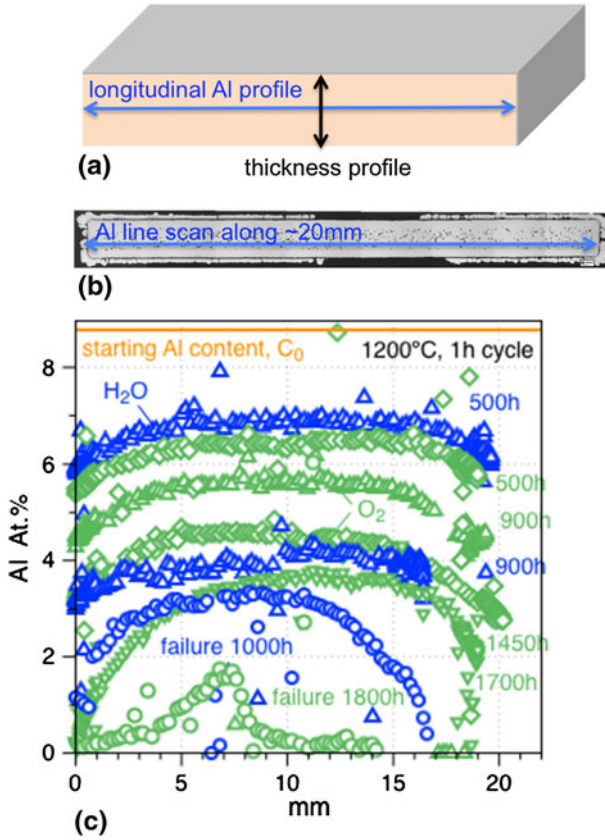
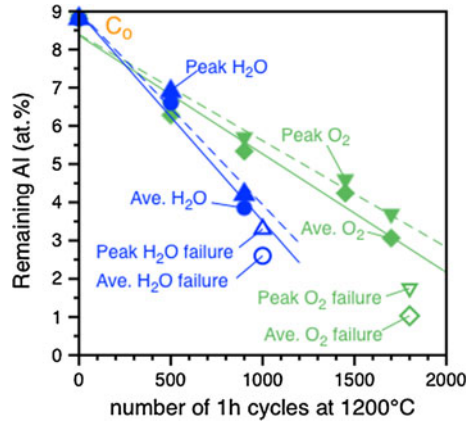


Fig. 6 **a** Schematic showing the EPMA line scan orientation, **b** example of EPMA line scan along the cross section of the specimen exposed to air + H₂O for 1,000, 1 h cycles at 1,200 °C, **c** Al profiles for ~1.5 mm thick MA956 specimens 1 h cycled for different durations in O₂ and air + 10 % H₂O at 1,200 °C

the specimen thickness at the specimen center [6, 14, 15]. The Al concentration gradients along the specimen length result in fact from higher Al consumption rates at the specimen edges, and above all at the corners, because of stress concentration and localized spallation during thermal cycling.

From Al profiles such as those shown in Fig. 6b, the peak and average Al contents were determined for alloy MA956, Fig. 7. Again, a linear relationship with exposure time was observed in both environments, with the Al content decreasing in air + 10 % H₂O twice as fast as in O₂, confirming the effect of H₂O on Al consumption. As expected, Al measurements from the specimens tested to breakaway oxidation do not fit well with the linear approximation from the interrupted test because of AlN formation. The estimation of oxidation lifetime from Al content, as suggested in the relationship in Eq. 1, currently neglects the reality that Al consumption is strongly influenced by specimen and component geometry. Integration of this factor will be discussed in subsequent papers.

Fig. 7 Peak and average Al contents from EPMA measurements along the length of ~ 1.5 mm thick MA956 specimens versus the cycle number for the same specimens



Porosity Formation in MA956

Cross sections of MA956 specimens cycled at 1,200 °C up to failure in three environments are shown in Fig. 8. Voids formation in the alloys occurred during exposure, with a higher volume formed in the CO_2 H_2O environment, including some local void coalescence Fig. 8d. Image analysis was used to estimate the amount of porosity and the range areal % porosity values obtained are listed adjacent to each image in Fig. 8. For all the specimens, a ~ 300 μm thick porosity-free region was noticeable beneath the oxide/alloy interface. Porosity formation in ODS alloys has been extensively studied and many authors concluded that porosity in ODS alloys can be attributed to the presence of micro-voids in the ball-milled ODS powder where gas is trapped during this fabrication step (likely Ar in the case of alloy MA956) [16 18]. However, internal voids have also been attributed to the selective oxidation of Al and the difference of diffusion coefficient between Al and Fe in FeCrAl alloys (or Al and Ni in NiCrAl [19]), leading to Kirkendall porosity [20]. Figure 8 suggests that the exposure environment also affects the void formation and that the internal fluxes of Al and Fe may not be the only mechanism involved.

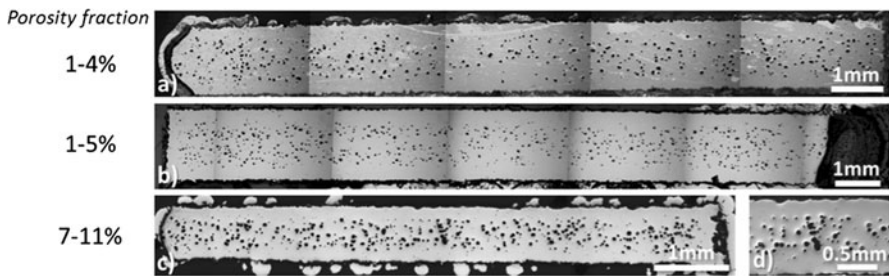
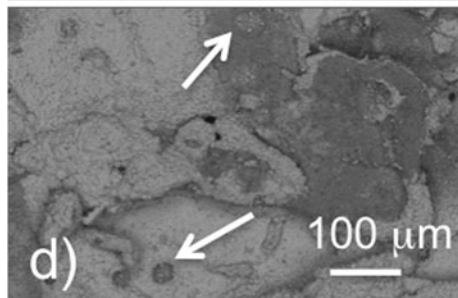
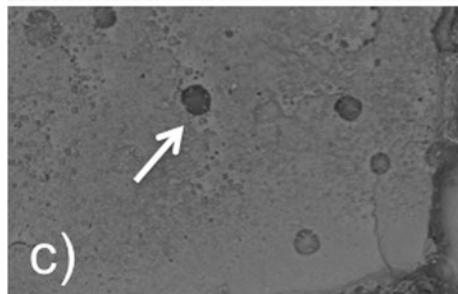
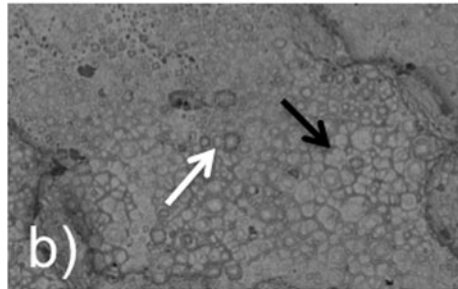
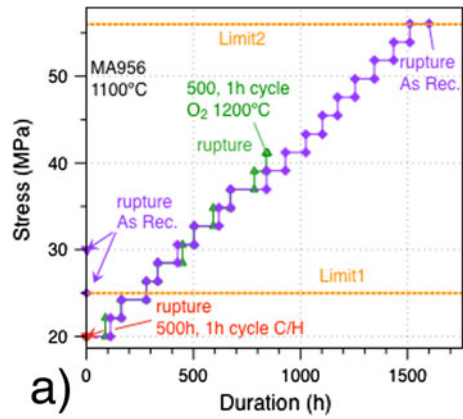


Fig. 8 Cross section along the length of MA956 specimens exposed at 1,200 °C, to 1 h cyclic testing **a** in O_2 for 1,800 cycles, **b** in air + 10 % H_2O for 1,200 cycles, **c**, **d** in the O_2 buffered mixture of 50 % CO_2 + 50 % H_2O for 1,150 cycles

Fig. 9 a Incremental creep testing of MA956 specimens at 1,100 °C for as received and pre exposed specimens for 500 1 h cycles in O₂ and O₂ buffered 50 % CO₂ + 50 % H₂O and fracture surfaces of **b** as received after 1,600 h, **c** O₂ exposed after 846 h, **d** O₂ buffered 50 % CO₂ + 50 % H₂O exposed that failed during loading to 20 MPa



Creep Testing

Incremental creep testing, where the stress is increased at regular intervals, is a convenient way to estimate the stress threshold in ODS alloys. Figure 9a shows the 1,100 °C creep results for MA956 with and without 500 h pre-oxidation exposures. The creep behavior of MA956 alloy is complicated, with two stress thresholds that need to be considered: the first ~25 MPa limit (L1) is the stress at which rupture occurred during loading or after only a few hours, and the significantly higher ~56 MPa limit (L2), corresponding to the stress at which rupture occurred after incremental increases of the stress, starting from a stress of 20 MPa (below L1). For pre-exposure in O₂, L2 decreased to 42 MPa and for pre-exposure in O₂-buffered 50 % CO₂ + 50 % H₂O, L1 decreased to less than 20 MPa. The fracture surfaces in Fig. 9b d, show the presence of large voids (white arrows) for the pre-oxidized specimens. Smaller voids developed during creep testing for 1,600 h at 1,100 °C, and the fracture surface appeared more ductile with dimples at the specimen surface (black arrow). Further analysis of the rupture mode is continuing to ensure that variations of creep properties are not related to specific microstructure features, such as the number of grains in given specimen or specific grain boundary orientation.

Conclusion

Accelerated 1 h cyclic oxidation testing at 1,200 °C conducted in O₂, and air + 10 % H₂O demonstrated a detrimental effect of H₂O on ODS FeCrAl oxidation resistance, with higher cyclic oxidation rates and shorter times to breakaway after oxidation in air + 10 % H₂O compared to exposure in dry O₂. Similar testing in O₂-buffered 50 % CO₂ + 50 % H₂O had less of an impact on oxide scale growth or lifetime, but resulted in increased formation of voids in MA956. Creep testing of pre-oxidized specimens revealed that exposure in O₂-buffered 50 % CO₂ + 50 % H₂O or O₂ appeared to affect creep lifetime. At 1,100 °C, the 50 % CO₂ + 50 % H₂O atmosphere had little effect on the oxidation behavior when 0.75 % O₂ was added as a buffer but, without O₂, a significant increase in spallation was observed compared to exposure in laboratory air. Finally, comparison of two batches of PM2000 highlighted significant differences in oxidation performance due to minor changes in the interstitial elements.

Acknowledgments The author wish to acknowledge G. Garner, T. Lowe, M. Stephens and J. Moser for assistance with the experimental work, as well as D. N. Leonard for EPMA analysis, M. Lance for stress measurement using the PSLS technique and K. Strader for the specimen porosity analysis. They also thank M. Brady, P. Tortorelli and I. Wright for reviewing the manuscript. This research was sponsored by the U.S. Department of Energy, Fossil Energy Advanced Materials Research Program.

References

1. J. C. Healy, M. Rees, J. D. Parker, R. C. Hurst, in *The proceedings of the Seventh International Conference on the Creep and Fracture of Engineering Materials and Structures*, Vol. 719 (University of California, Irvine, CA, 1997).

2. W. J. Quadackers and K. Bongartz, *Materials and Corrosion* **45**, 232 (1994).
3. J. R. Nicholls, R. Newton, N. J. Simms and J. F. Norton, *Materials at High Temperatures* **20**, 93 (2003).
4. H. Al Badairy and G. J. Tatlock, *Materials at High Temperatures* **17**, 133 (2000).
5. A. Kolb Telieps, U. Miller, H. Al Badairy, G. J. Tatlock, D. Naumenko, W. J. Quadackers, G. Strehl, G. Borchardt, R. Newton, J. R. Nicholls, M. Maier and D. Baxter, *European Federation of Corrosion publications* **34**, 123 (2001).
6. A. Vande Put, S. Dryepont and B. A. Pint, *NACE Paper 19608, Houston, TX, presented at NACE Corrosion 2010* (Houston, TX, 2011).
7. R. Janakiraman, G. H. Meier and F. S. Pettit, *Metallurgical and Materials Transactions A* **30**, 2905 (1999).
8. S. Hayashi and T. Narita, *Oxidation of Metals* **56**, 251 (2001).
9. M. C. Maris Sida, G. H. Meier and F. S. Pettit, *Metallurgical and Materials Transactions A* **34**, 2609 (2003).
10. B. A. Pint, J. A. Haynes, Y. Zhang, K. L. More and I. G. Wright, *Surface and Coatings Technology* **201**, 3852 (2006).
11. B. A. Pint and I. G. Wright, *NACE Paper 10 198, Houston, TX, presented at Corrosion 2010* (San Antonio, TX, 2010).
12. C. Mennicke, E. Schumann, C. Ulrich and M. Rühle, *Materials Science Forum* **251–254**, 389 (1997).
13. J. Smialek, *Materials Science Forum* **595–598**, 191 (2008).
14. I. G. Wright, R. Peraldi and B. A. Pint, *Materials Science Forum* **461**, 579 (2004).
15. L. Marechal, B. Lesage, A. M. Huntz and R. Molins, *Oxidation of Metals* **60**, 1 (2003).
16. Y. L. Chen and A. R. Jones, *Metallurgical and Materials Transactions A* **32**, 2077 (2001).
17. Y. L. Chen, A. R. Jones and U. Miller, *Metallurgical and Materials Transactions A* **33**, 2713 (2002).
18. M. Turker, *Journal of Materials Science* **40**, 1201 (2005).
19. V. Provenzano, K. Sadananda, N. P. Louat and J. R. Reed, *Surface and Coatings Technology* **36**, 61 (1988).
20. G. Merceron, R. Molins and J. L. Strudel, *Materials at High Temperatures* **17**, 149 (2000).